DECAY PROCESSES OF HIGH-FREQUENCY NONEQUILIBRIUM PHONONS IN PRASEODYMIUM-DOPED LASER CRYSTALS

Wang Xiaojun[a] Dennis W M[b] Yen W M[b]

[a] (*Department of Physics & Astronomy, Georgia Southern University, Statesboro, GA* 30460, *USA*)

[b] (*Department of Physics and Astronomy, The University of Georgia, Athens, GA* 30502, *USA*)

Abstract

We have investigated the decay of nonequilibrium phonons in YAG Pr^{3+} (1.0at.%) and $LiYF_4$ Pr^{3+} (1.0at.%) at a temperature of 9K. Nonequilibrium phonon populations at 43.0, 51.9, 66.0 and 113cm^{-1} are generated monochromatically with a high-power pulsed far-infrared laser using defect-induced one-phonon absorption, and their temporal and spectra evolution determined using a time-resolved vibronic sideband spectrometer. We find that two decay mechanisms dominate the nonequilibrium phonon relaxation in the crystals: anharmonic decay via three-phonon interactions and two-phonon-one-electron inelastic-scattering processes. In $LiYF_4$ system, we observe the broad band distribution that results from the anharmonic decay of the initial monochromatic phonon population. In YAG system, the latter mechanism leads to the evolution of a highly peaked phonon distribution that persists for several phonon generations.

Key words nonequilibrium phonons, high-frequency phonons, lattice dynamics, YAG, YLF

1 INTRODUCTION

In a real crystal system, the lattice vibrations will not be the eigenstates of the system, i.e., an initially monochromatic nonequilibrium phonon population will decay after it is generated. The decay behavior of the nonequilibrium phonons provides a basic understanding of the phonon relaxation mechanisms. Theoretical studies have shown that anharmonic interactions that involve three phonons dominate the relaxation of monochromatic high-frequency nonequilibrium phonons. Anharmonic decay rates of high-frequency acoustic phonons were first studied by Slonimskii[1] using nonlinear elasticity theory. He performed calculations for an isotropic dispersionless solid and showed that longitudinal phonons can split into two lower frequency phonons and have a decay rate which increases as ^{5}. These predictions have been theoretically confirmed by Kle-

Received 1 August 1998

mens and Orbach et al[2,3] and have been supported by a large body of experimental work[4~9]. However, due to the limitations of the techniques for high frequency phonon generation and detection, the initial products from the decay of a monochromatic phonon distribution have not been previously observed. The phonon distributions which occur shortly after the generation of monochromatic phonons and before the onser of scaling behavior[4] provide additional information on the phonon decay processes.

In many systems, on the other hand, high-frequency acoustic phonons are strongly scattered or trapped by the low-energy electronic transitions[10,11]. These processes can dominate the anharmonic interactions, lead to the evolution of a highly peaked phonon distribution, and result in the deviation of the phonon lifetime from $^{-5}$. In this paper, the combination of phonon generation by defect-induced one-phonon absorption (DIOPA) with an absorption vibronic sideband phonon spectrometer (AVSPS) was used to determine the temporal and spectral evolution of nonequilibrium phonons in the Pr^{3+} $LiYF_4$(YLF) and Pr^{3+} YAG systems. Anharmonic interaction and inelastic scattering were found to dominate nonequilibrium phonon relaxation in the two systems respectively.

2 EXPERIMENT

The samples used in the experiments are $3\times3\times6$ mm^3 YAG Pr^{3+}, (1 at.% where at. means atomic weight) and $2\times4\times6$ mm^3 YLF Pr^{3+} (1 at.%) single crystals. The samples were polished with 0.3 m alumina and oil.

A schematic of the experimental configuration for phonon studies is shown in Fig. 1. The sample was mounted on the cold finger of a RMC E22 two-stage closed-cycle refrigerator. Far-infrared radiation covering a range of frequencies was generated using a superradiant cell pumped by a CO_2 laser. The FIR was focused by an off-axis parabolic reflector producing a 2-mm spot at the sample. The Nd YAG laser pumped dye laser probe and the FIR beams are incident on the sample in a co-linear and counter-propagating geometry, with the phonon-induced fluorescence collected at 90 degrees to the pump and detection beams. After spectral filtering using a 0.85m double spectrometer, the signal was detected by an RCA C313034A-02 photomultiplier tube (PMT) in a water cooled radio-frequency-interference shielded housing, and amplified by a Philips 100 MHz, $\times$100 amplifier. Finally the signal was sent to a Stanford Research SR400 photon counter controlled by a computer.

Synchronization of the FIR and optical pump-probe lasers and the fluorescence detection is presented in Fig. 2. The master clock for the timing sequence was the 10Hz oscillator of the Nd YAG laser. A delayed pulse, synchronous with the firing of the Nd YAG flashlamps, triggered the Stanford Research Systems DG535 multi-delay generator. Channel 1 triggered the Nd YAG Q-switch at a delay of 230ms which was cho-

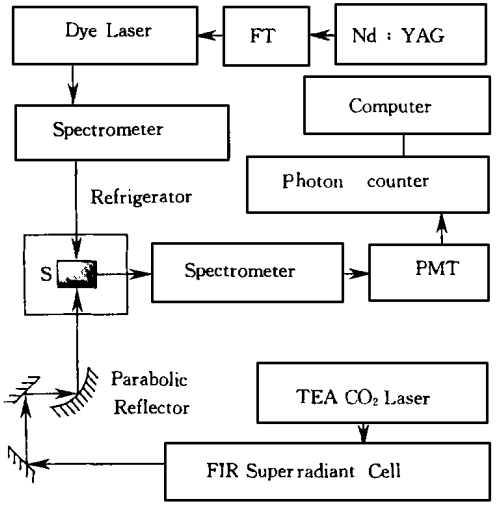

FT: Frequency Tripling crystal; S: Sample

Fig. 1 A schematic of the experimental setup.

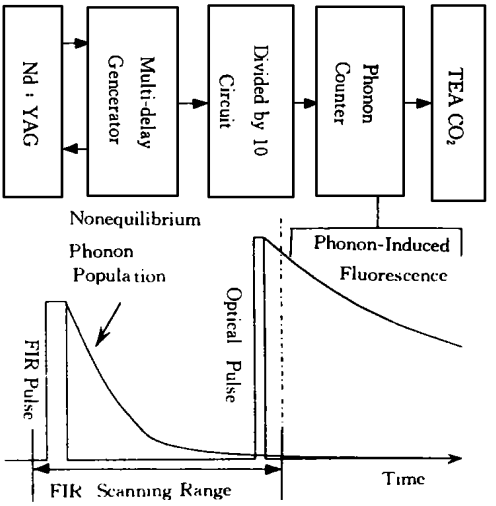

Fig. 2 Time scheme for the pump-probe experiment. Optical probe laser is fixed while the FIR is delayed by the photon counter gate B.

sen to maximize the dye laser power. A second delay from channel 2 triggered a divide by 10 circuit which provided 1Hz trigger pulses for the dual gated photon counter. Gate A of the photon counter was used for data acquisition and gate B was used in scanning mode as a variable delay trigger for the CO_2 laser. The delay range and increment rate were chosen to give the desired pump-probe delay and signal averaging time, respectively. Negative pump-probe delays, i.e., the optical detection pulses arrived earlier than FIR generation pulses at the sample, gave a signal baseline due to the thermal phonons, which was used to calibrate each phonon transient at this temperature. The fluorescence collection gate (A) was fixed with respect to the probe pulse and started several microseconds after the largest negative pump-probe delay to prevent noise counts from appearing on the baseline. The radio frequency interference noise was produced by CO_2 laser spark gap and occurred about 1.1ms earlier than the FIR light pulse. The gate duration was set at 1.5 to 2 e-foldings of the $^3P_0$ lifetime in Pr^{3+}-doped YAG and YLF, which are 14 and 52 s respectively at a temperature of 9K.

An anti-Stokes calibration of the nonequilibrium phonon population can be obtained when the dye laser pulse is incident on the sample before the FIR pulse. The nonequilibrium occupation number at frequency , $n_{non}(\ )$, then can be calculated by

$$n_{non}(\ ) = n_{th}(\ ) \frac{(\ _0 - \ ) - \ _{th}(\ _0 - \ )}{\ _{th}(\ _0 - \ )}. \quad (1)$$

$n^{non}(\ )$ is the thermal occupation number at phonon energy , which is given by the Bose-Einstein distribution. $(\ _0 - \ )$ and $_{th}(\ _0 - \ )$ are the phonon-induced absorption

coefficients to the $^3P_0$ zero-phonon line at energy $_0$ in the presence of a nonequilibrium phonon population and a thermal phonon population, respectively. The absorption coefficients $_{th}(\ _0-\ )$ and $(\ _0-\ )$ are obtained from the total time-integrated phonon-induced fluorescence detected by the optical probe pulse before and after the FIR generation pulse, respectively. Arbitrary phonon numbers $N_{non}(\ )$ can be calculated from phonon occupation numbers by multiplying by ^{2} according to the Debye approximation.

3 RESULTS AND DISCUSSION

The fluorescence spectra from 470 to 670nm for both Pr^{3+} YLF and Pr^{3+} YAG measured at 9K are shown in Fig. 3. The $^3P_0$-$^3F_2$ transition (639.4nm) and $^3P_0$-$^3H_6$ (616.1nm) transition are used as monitors to detect the phonon-induced fluorescence in the two systems respectively. The insets show the decay behaviors of the corresponding emissions from the transitions.

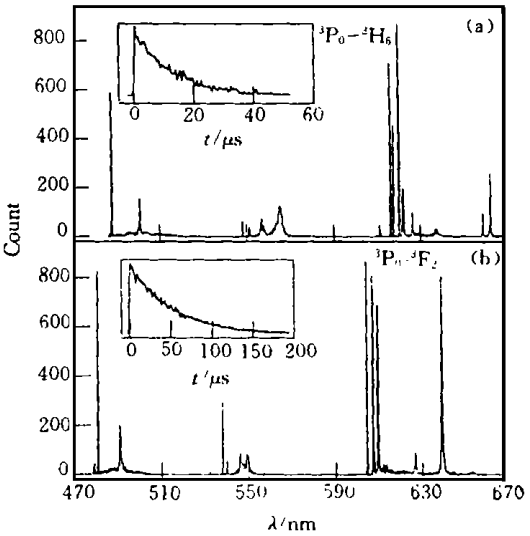

Fig. 3 Emission spectra of Pr^{3+} in YAG (3a) and YLF (3b) at 9K. The insets show transients of $^3P_0$ level. Phonon-induced absorption is measured by monitoring the fluorescence from the labeled transitions.

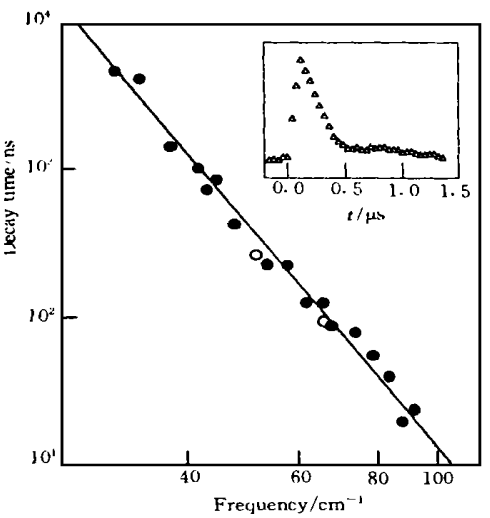

Fig. 4 Frequency dependence of the phonon decay time. The solid line represents the $^{-5}$ dependence expected from the isotropic dispersionless model. The open circles show the decay times of monochromatically generated phonons at 51.9 and 66.0 cm^{-1}. Solid circles show that of the decay products from a 113cm^{-1} monochromatic phonon population.

Fig. 4 shows the frequency dependence of phonon decay times in Pr^{3+} YLF. The phonon decay time at each frequency is obtained from phonon transients measured by varying the time separation between the FIR phonon generation and optical detection. The open circles are measured with monochromatically generated phonons, i.e.,

= $_g$, the FIR frequency. The filled circles are measured from the lifetimes of decay products of $_g$= 113cm^{-1} phonons. The solid line represents the best fit to

$$\frac{1}{_d} = A \quad ^5, \tag{2}$$

where A is a constant and is a measure of the anharmonicty. This relationship is a direct consequence of the assumption that the system is an isotropic, dispersionless Debye crystal. For phonons with a given frequency , the probability function for phonon decay due to anharmonic interaction from into two daughter phonons, and − , will be ^{2}(−)^2. Integration of all the possible decay products will yield the ^{5}decay rate, as expressed in Eq. (2).

The inset in Fig. 4 shows a typical resonant phonon transient of $_g$= 66cm^{-1}. The phonon spectral distribution at a given time can be obtained by scanning the detection frequency (optical laser detuning), while the delay of the optical gate is fixed. In practice, however, time-resolved phonon spectra are constructed from a set of phonon transients at different fixed frequencies. Fig. 5 shows the phonon spectral distribution respectively at 40, 400, and 800ns after the monochromatic generation at 51.9 cm^{-1}.

Time-resolved phonon spectra obtained with initial monochromatic phonon generation at 43.3 cm^{-1} in Pr^{3+} YAG system is shown in Fig. 6. The strong build up of narrow-band phonon population at both 23 and 43 cm^{-1} is observed.

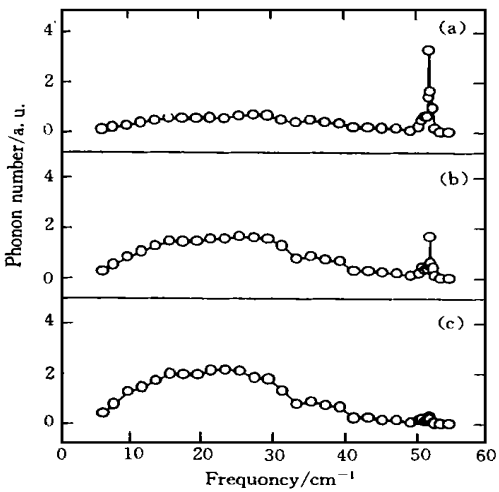

Fig. 5 Temporal and spectral evolution of monochromatic phonons generated at 51.9 cm^{-1}. (a), (b) and (c) correspond to the spectra at 40, 400 and 800 ns, respectively.

In interpreting the phonon spectra it is necessary to consider the details of the excitation spectrum of $^3P_0$ level shown in Fig. 7(a). In addition to the previously reported crystal-field split lines at 19 and 50 cm^{-1} two peaks at 23 and 43 cm^{-1} are observed. The absence of similar peaks on the Stokes side of the zero-phonon transition suggests that they are not due to low-lying optical phonons. Pumping of the $^3P_0$ from these states at 9K produces fluorescence spectra that are similar to that of the undistorted Pr^{3+} ions in general. These peaks therefore are believed to be due to either electronic levels in the ground-state manifold of Pr^{3+} ions which are located in distorted sites or alternatively Pr^{3+} pair states.

Evolution of the narrow-band phonon distributions can be understood in terms of inelastic scattering of the initial monochro-

matic phonons from the 23 and 43cm^{-1} states. As shown in Fig. 7(b), a phonon of frequency $_{ph}$ enters a two-level system with the excited state associated with the distorted ions and causes an electronic transition of frequency , yielding a phonon with the different frequency $_{ph}-$. he electronic excitation then relaxes by rapid one-phonon emission to yield a phonon of frequency . This two-phonon one-electron Raman process can well explain the phonon evolution with a highly peaked distribution.

In Pr^{3+} YLF, there are no low-lying electronic levels in the frequency range of our investigation. The low phonon scattering rate combined with a comparatively high Debye frequency[12] thus makes this an ideal system to investigate purely anharmonic interactions[13].

The variation of phonon lifetime with generation frequency in Pr^{3+} YAG is shown in Fig. 8. The observed dependence of $_d$ on is weaker than $^{-5}$ and appears to asymptotically tend toward $^{-2}$[10]. This behavior can be understood as follows.

In the presence of strong inelastic sctering, an additional channel for nonequilibrium phonon decay is introduced and the phonon lifetime should deviate from the frequency dependence expected for anharmonic decay. For nonresonant Raman scattering of high-frequency phonon from low-lying electronic levels, the decay rate may be expressed as[14]

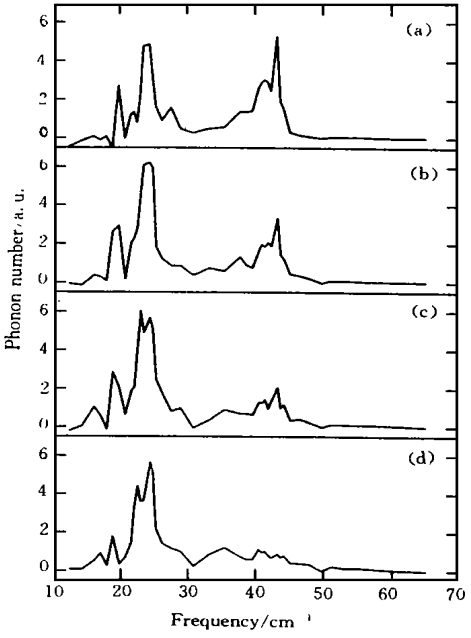

Fig. 6 Time-resolved phonon spectra after monochromatic phonon generation at 43.3 cm^{-1}. (a), (b), (c) and (d) correspond to the delay time at 100, 600, 1100 and 2400ns, respectively.

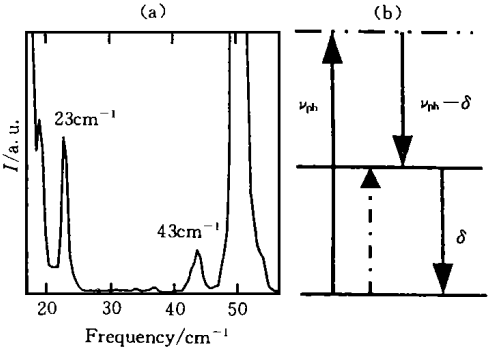

Fig. 7 (a) Anti-Stokes excitation spectrum of $^3P_0$ at 9K by monitoring the $^3P_0-{}^3H_6$ fluorescence. (b) A schematic diagram of inelastic scattering.

$$\frac{1}{_{d}^{inel}} \propto (- _i)^3, \qquad (3)$$

where $_i$ is the energy of the electronic level. The phonon decay rate associated with inelastic scattering from all the electronic levels can be written

$$\frac{1}{\tau_{inel}} = \sum_i b_i (\omega - \omega_i)^3 \theta_i, \qquad (4)$$

where θ_i is a step function which is equal to 1 for $\omega \geq \omega_i$ or 0 for $\omega < \omega_i$. That is, at low temperatures when the occupation of the excited electronic levels is low, it is assumed that the electronic level of ω_i will only scatter the phonons with energy above this level. The phonon decay time due to the two relaxation mechanisms can then be expressed as follows:

$$\tau_d = \frac{1}{a\omega^5 + \sum_i b_i (\omega - \omega_i)^3 \theta_i}. \qquad (5)$$

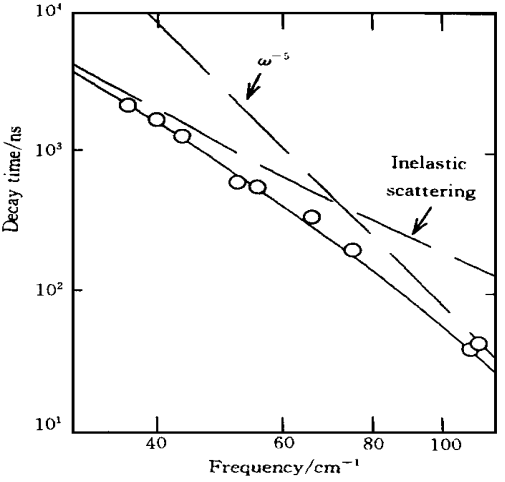

Fig. 8 Phonon decay time vs phonon frequency. Solid curve is the best fit of Eq. (5) to the data. The dashed lines show the respective contributions of anharmonic and inelastic scattering processes to the phonon decay.

Constants a and the b_i can be treated as adjustable parameters when the equation is fitted to experimental date. It was not possible to obtain a good fit to the data by considering $\omega_1 = 23$ and $\omega_2 = 43$ cm^{-1} alone. The fit shown in Fig. 8 is obtained from Eq. (5) by considering an additional low energy state (10cm^{-1} in our calculation). It was not possible to observe a peak in this frequency range due to the reduced detection sensitivity at low frequencies. Parameters a and b_i are determined to be $a = 1.3 \times 10^{-3}$ (cm^{-1})$^{-5}$s^{-1}, $b_1 = b_2 = 1.3 \times 10^2$ (cm^{-1})$^{-2}$s^{-1}, and $b_3 = 3.3 \times 10^2$(cm^{-1})$^{-2}$s^{-1}. b_1, b_2 and b_3 correspond to the contributions from electronic states at $\omega = 23, 43$ and 10 cm^{-1} respectively. The fact that b_3 is greater than both b_1 and b_2 may indicate that the inelastic scattering is from several electronic states at low frequencies.

One other explanation for the deviation of the phonon lifetime from ω^{-5}, especially at lower frequencies, is that the phonons are leaving the interaction volume by quasidiffusive processes (i.e., low frequency phonons have a larger diffusion constant than high frequency phonons due to Rayleigh scattering). If this occures, the total nonequilibrium phonon energy would decrease over the detection time.

Based on the Debye approximation, the total energy as a function of time can be obtained by

$$E_{TOT}(t) = A \int_0^g n(t, \omega) \omega^3 d\omega. \qquad (6)$$

$E_{TOT}(t)$ is plotted against detection time in Fig. 9, where a nearly constant $E_{TOT}(t)$ is found over the experimental timescale. This indicates that the phonons with lower frequency do not move out the volume due to the strong scattering from the impurities at

distorted sites. This is consistent with the phonon transport results discussed in the following chapter, where it is shown that a substantially longer time is needed for nonequilibrium phonons to move out of the detection volume.

It is noted that the anharmonic decay times in YAG are substantially longer than those observed previously in LaF_3[5]. This reduction in decay rate can be accounted for by the higher Debye frequency in YAG[15, 16]. The phonon decay rates in YAG would be much longer if there were no impurities doped into the crystal. This is in agreement with thermal conductivity studies in pure YAG[15] in which the thermal conductivity becomes dependent on the sample size for $T < 30$ K, i.e., the dominant scattering mechanism is boundary scattering[17].

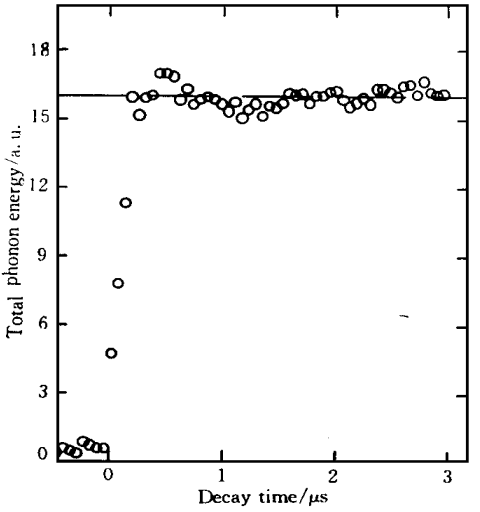

Fig. 9 Time dependence of total phonon energy obtained by integrating over all frequencies of nonequilibrium phonons. Dashed line is a time average of total phonon energy.

4 CONCLUSIONS

Two decay mechanisms have been observed and discussed. They are (1) anharmonic decay that at low temperature yields a ^{5} frequency dependent decay rate, and (2) relaxation due to the inelastic scattering from the ions at highly distorted sites. In the case of Pr^{3+} YLF, anharmonic interaction dominates the decay processes with broadband phonon distribution. In the case of Pr^{3+} YAG, the phonon decay rate deviates from ^{5}, especially at lower frequencies. The inelastic scattering leads to a highly peaked phonon distribution that persists for times much greater than the lifetime of the initial monochromatic phonons.

REFERENCES

[1] Slonimskii G L. Zh. Eksp. Teor. Fiz., 1937**7**, 1457(JETP 7).
[2] Orbach R, Vredevoe L A. Physics(Long Island City, NY), 1964, **1**, 91.
[3] Klemens G. J. Appl. Phys., 1967, **38**: 4573.
[4] Yang H S, Kirkpatrick S M, Dennis W M. J. Jumin., 1998, **76/77**: 540.
[5] Tolbert W A, Dennis W M, Yen W M. Phys. Rev. Lett., 1990, **65**: 607.
[6] Wang Xiaojun, Dennis W M, Yen W M. Phys. Rev. Lett., 1991, **67**: 2807.
[7] Wang Xiaojun, Dennis W M, Yen W M. J. Lumin., 1992, **53**: 44.

[8] Meltzer R S, Rives J E, Dixon G S. Phys. Rev., 1983, B**28**: 4786.
[9] Baumgartner R, Engelhardt M, Renk K F. Phys. Rev. Lett., 1981, **47**: 1403.
[10] Wang Xiaojun, Ganem J. Dennis W M *et al*, Phys. Rev. 1991, B **44**: 900.
[11] Yom S S, Meltzr R S, Rives J E. Phys. Rev. 1987, B**36**: 6664.
[12] Blanchfield P, Saunders G A. J. Phys., 1979, C **12**: 4673.
[13] Wang Xiaojun, Dennis W M, Yen W M. Phys. Rev., 1992, **46**: 8168.
[14] Kaplyanskii A A, Basun S A. Nonequilibrium Phonons in Nonmetallic Crystals(North-Holland, Amsterdam, 1986), chap 8.
[15] Slack G A, Oliver D W. Phys. Rev., 1971, B**4**: 592.
[16] Kushida T. Phys. Rev., 1969, **185**: 500.
[17] Thacher P D. Phys. Rev., 1967, **156**: 975.